Bioelectrochemistry 157 (2024) 108675

Contents lists available at ScienceDirect

Bioelectrochemistry

journal homepage: www.journals.elsevier.com/bioelectrochemistry

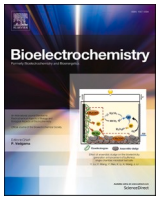

The organo-metal-like nature of long-range conduction in cable bacteria

Dmitrii Pankratov [a,b], Silvia Hidalgo Martinez [a], Cheryl Karman [a,b], Anastasia Gerzhik [c], Gabriel Gomila [d,e], Stanislav Trashin [b], Henricus T.S. Boschker [a,f], Jeanine S. Geelhoed [a], Dirk Mayer [c], Karolien De Wael [b], Filip J.R. Meysman [a,f,*]

[a] Geobiology Group, Microbial Systems Technology Excellence Centre, Department of Biology, University of Antwerp, Universiteitsplein 1, B-2610 Wilrijk, Belgium
[b] A-Sense Lab, Department of Bioscience Engineering, University of Antwerp, Groenenborgerlaan 171, B-2020 Antwerpen, Belgium
[c] Institute of Biological Information Processing, Bioelectronics (IBI-3), Forschungszentrum Jülich, 52428 Jülich, Germany
[d] Nanoscale Bioelectric Characterization Group, Institute for Bioengineering of Catalunya (IBEC), The Barcelona Institute of Science and Technology, Baldiri i Reixac 15-21, 08028 Barcelona, Spain
[e] Department of Electronics and Biomedical Engineering, Universitat de Barcelona, Martí i Franqués 1, 08028 Barcelona, Spain
[f] Department of Biotechnology, Delft University of Technology, Van der Maasweg 9, 2629HZ Delft, the Netherlands

ARTICLE INFO

Keywords:
Cable bacteria
Long-distance electron transport
Protein conductivity
Electrochemical impedance spectroscopy
Bioelectronics

ABSTRACT

Cable bacteria are filamentous, multicellular microorganisms that display an exceptional form of biological electron transport across centimeter-scale distances. Currents are guided through a network of nickel-containing protein fibers within the cell envelope. Still, the mechanism of long-range conduction remains unresolved. Here, we characterize the conductance of the fiber network under dry and wet, physiologically relevant, conditions. Our data reveal that the fiber conductivity is high (median value: 27 S cm^{-1}; range: 2 to 564 S cm^{-1}), does not show any redox signature, has a low thermal activation energy (E_a = 69 ± 23 meV), and is not affected by humidity or the presence of ions. These features set the nickel-based conduction mechanism in cable bacteria apart from other known forms of biological electron transport. As such, conduction resembles that of an organic semi-metal with a high charge carrier density. Our observation that biochemistry can synthesize an organo-metal-like structure opens the way for novel bio-based electronic technologies.

1. Introduction

Electron transport across proteins is fundamental to biology, and typically occurs through sequential hopping of electrons between closely spaced cofactors (such as hemes, FeS clusters or quinones). This multi-step electron transport is well known from the electron transfer chain in mitochondria or the photosynthetic system in chloroplasts, but overall, the length scale of conduction that occurs in these membrane proteins is limited to <20 nm [1]. The recent discovery of cable bacteria demonstrates that electron transport in proteins may greatly surpass this nanometer scale [2,3]. These multicellular bacteria mediate nano-ampere currents across centimeter distances through an internal protein fiber network [4,5], thus inducing a quantum leap in the range of biological electron transport [2,6,7]. As protein materials are generally thought to be poorly electrical conductors, this raises the question of how such extremely efficient, long-range conduction is possible through a biological proteinaceous structure.

Cable bacteria form centimeter-long filaments that channel electrons from cell to cell across a linear chain of >10,000 cells [2,6,7]. This capability equips them with a competitive advantage for harvesting electron donors in the anoxic zone of aquatic sediments [3]. To mediate electrical currents across centimeter distances, cable bacteria contain a parallel network of protein fibers (~50 nm diameter) within their cell envelope [8], which form a unique and extremely long conductive relay network for electron transport [5,9]. These fibers have been shown to consist of a conductive core with a nickel-containing metalloprotein and an outer nonconductive shell (Fig. 1), but the detailed molecular structure remains presently unresolved [4]. The fibers do show exceptional electrical properties: the *in vivo* current density is comparable to that of copper wiring, and the fiber conductivity rivals that of the most performant man-made organic conductors, including highly doped conjugated polymers [5,10]. This way, cable bacteria demonstrate that

* Corresponding author at: Geobiology Group, Microbial Systems Technology Excellence Centre, Department of Biology, University of Antwerp, Universiteitsplein 1, B-2610 Wilrijk, Belgium.
E-mail addresses: filip.meysman@uantwerpen.be, f.j.r.meysman@tudelft.nl (F. J.R. Meysman).

https://doi.org/10.1016/j.bioelechem.2024.108675
Received 31 October 2023; Received in revised form 22 February 2024; Accepted 24 February 2024
Available online 25 February 2024

biological evolution has crafted protein structures that can support highly efficient electron conduction, which holds promise for novel biotechnological and bio-electronic applications.

However, the question as to how the protein fibers in cable bacteria enable such extraordinary conduction remains fundamentally unresolved. To get insight into the conduction mechanism, we performed a detailed electrical characterization of the conductive fiber network in the dry state as well as in ionic solutions representative for electron transport under *in vivo* conditions. Our data reveal that the conduction mechanism in cable bacteria lacks the expected redox signature that is conventionally seen in metalloproteins involved in biological electron transport. Instead, several organo-metal-like features emerge, suggesting high carrier densities and delocalization, which set the conduction mechanism fundamentally apart from other known forms of biological electron transport.

2. Materials and methods

2.1. Materials

All chemicals were of analytical grade and used without further purification. Aniline, ethylenediaminetetraacetic acid, sodium dodecyl sulphate (SDS), 6-mercapto-1-hexanol, $K_4[Mo(CN)_8]$, $[Ru(NH_3)_6]Cl_3$, $Na_2HPO_4{\cdot}2H_2O$, $NaH_2PO_4{\cdot}H_2O$, NaCl, KCl, H_3PO_4, H_2SO_4, HCl, NaOH were purchased from Sigma-Aldrich. Multiwalled CNTs "Taunit M" (with the outer and inner diameters of 8–15 and 4–8 nm, respectively; length $\geq$ 2 μm) were obtained from NanoTechCenter Ltd. (Tambov, Russia). The composite PANI/CNT was obtained by *in situ* chemical polymerization of aniline following a previously adapted protocol [11]. A mass of 1.7 mg of CNTs or PANI/CNT composite was ultrasonicated in 0.75 mL of ethanol for 15 min. A volume of the obtained suspension (10 μL) was dropcast onto the surface of an interdigitated gold electrode (IGE) and dried (see below). The electrolyte solution employed in electrochemical gating, cyclic voltammetry and electrochemical impedance spectroscopy (EIS) measurements was 50 mM phosphate buffer (pH 7.0) containing 0.1 M KCl, if not specified otherwise.

2.2. Sample preparation

Cable bacteria cultivation and fiber skeleton extraction was performed by following previously developed protocols [5,8]. Briefly, surface marine sediment was collected from the creek bed within the Rattekaai salt marsh (51°26′21.6″N, 4°10′08.3″E) and was sieved, homogenized and repacked into PVC core liner tubes. The sediment cores were incubated in artificial seawater in the dark for several weeks until the typical fingerprint of cable bacteria metabolism was detected by microsensor profiling [12]. Individual filaments of cable bacteria were picked under a stereomicroscope with custom-made glass hooks and consecutively washed in several droplets of deionized water. Extraction of the fiber skeletons was performed by sequential treatment with aqueous solutions of SDS (1 % (w/w)) and sodium ethylenediaminetetraacetate (1 mM, pH 8). Fiber skeletons were washed with deionized water 6 times and transferred to the electrodes immediately after extraction. All solutions were prepared using deionized water (18.2 MΩ cm) produced with an Arium system (Sartorius, Germany).

2.3. Preparation of interdigitated gold electrodes

Interdigitated gold electrodes (IGEs; 125 × 2 digits, 6.76 mm in length with bands/gaps of 10 μm) were purchased from Metrohm DropSens (Spain). IGEs were sequentially cleaned by ultrasonication in ethanol (75 % v/v, 3 min) and water (3 min) and by electrochemical cycling in 0.5 M H_2SO_4 from −0.2 to 1.7 V vs saturated calomel electrode (SCE) with a scan rate of 0.1 V s^{-1} until steady-state

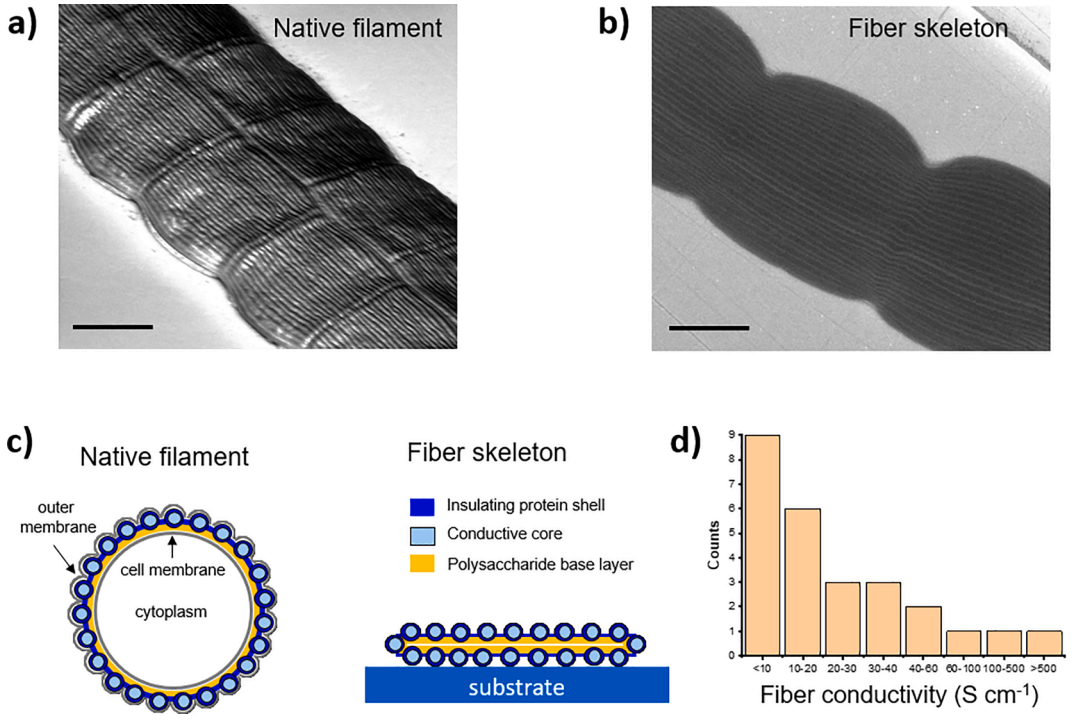

Fig. 1. The conductive fiber network in cable bacteria. a) Scanning electron microscopy of a small segment from a dry native cable bacterium filament (2 parallel filaments side by side). The outer surface shows the ridges which embed the conductive fibers. Electron beam energy: 1 kV, working distance: 4.1 mm, tilt: 52°, scale bar = 2 μm. b) Scanning electron microscopy micrograph of a dried fiber skeleton. A parallel network of fibers emerges (bright lines) indicating higher conductivity. Electron beam energy: 15 kV, working distance: 4.0 mm, tilt: 0°, scale bar = 2 μm. c) Fiber skeletons are obtained from native cable bacterium filaments through sequential chemical extraction, which removes the lipid membranes and cytoplasm. Cross-section schematics are shown for both a native filament and a fiber skeleton. Figure adapted from Boschker et al. [4] d) Histogram of fiber conductivities calculated from *I/V* curves recorded for fiber skeletons under dried conditions (N = 26 specimens).

voltammograms were obtained. The electrodes were rinsed with deionized water, incubated for 24 h in 8 mM solution of 6-mercapto-1-hexanol, washed with deionized water and dried. In the electrochemical gating experiment, bundles of fiber skeletons, CNTs or PANI/CNT composite were deposited on the surface of the thiol-modified IGE from the droplet and dried in the flow of argon.

2.4. Electrochemical measurements

All electrical and electrochemical measurements were carried out using PalmSens3 bipotentiostat and PalmSens4 potentiostat (Palmsens BV, Houten, the Netherlands), controlled by the PSTrace software.

2.4.1. Electrochemical gating of fiber skeleton bundles

Multiple fiber skeletons ("bundles") were deposited on IGEs thus forming many connections between the digits (Fig. 2). Measurements were performed with IGEs in an electrochemical cell with a solution volume of 40 mL using the bipotentiostat to conduct voltammetry sweeps. The source and drain served as two working electrodes, a glassy carbon rod and SCE were used as counter and reference electrodes, respectively (Fig. 2). Reported data were obtained for five independent IGE replicates.

2.4.2. Characterization of individual fiber skeletons

An individual fiber skeleton was first deposited onto a non-conductive microscope glass slide (Fig. 3). To ensure electrical contact, the terminal ends of the fiber skeleton were covered with conductive carbon paste (EM-Tec C30, Micro to Nano, the Netherlands) and waterproofed with an additional layer of nail polish (nitrocellulose dissolved in a solvent in ethyl acetate, Rimmel London, UK). To create the third electrical contact point, a drop of carbon paste was deposited in the middle of the fiber skeleton and waterproofed with an additional layer of nail polish (Fig. S2a). The electrical contact between the carbon paste and the potentiostat was generated by strips of copper tape (Fig. 3). Current (I)-voltage (V) curves were obtained in a two-electrode configuration by recording cyclic voltammograms between 0.2 and −0.2 V at a 10 mV s^{-1} scan rate. Single-filament EIS experiments were performed in a two-electrode configuration at 0 V with voltage amplitude perturbation of 5 mV over a frequency range of 500 kHz-10 Hz. EIS parameters were obtained by fitting the impedance spectra ($\chi^2 < 10^{-2}$ for all experiments) using the equivalent circuits presented in Fig. 4.

2.4.3. Temperature dependence of conductance of fiber skeleton bundles

Temperature dependence of conductance was investigated by EIS in a thermostated water-jacketed electrochemical cell with a volume of solution of 45 mL. Multiple fiber skeletons were deposited as a "bundle" onto the IGE as described above. EIS was performed in a three-electrode configuration using SCE and a glassy carbon rod as reference and counter electrodes, respectively, at 0 V with voltage amplitude perturbation of 5 mV over a frequency range of 60 kHz-0.5 Hz. EIS parameters were obtained by fitting the impedance spectra ($\chi^2 < 10^{-3}$ for all experiments) using the $R(QR)$ equivalent circuit. Reported data were obtained with three independent IGE replicates.

2.5. Fiber conductivity calculation

The fiber conductivity was calculated from I/V profiles of individual fiber skeletons using the equation (1):

$$\sigma = (\Delta I/\Delta V) \bullet (l/A) \text{ or equally } \sigma = (1/R_p) \bullet (l/A), \quad (1)$$

where $\Delta I/\Delta V$ is the slope of the I/V curve, or alternatively, R_p is the resistance obtained from fitting the EIS data. In this, l represents the measured length of the fiber skeleton segment between the electrical contacts, and A is the cross-sectional area of one conductive fiber (assumed to be 0.12 μm^2 for 60 fibers of 50 nm diameter [8]).

2.6. Equivalent electrical circuits

Fitting of the equivalent electrical circuits to impedance data was performed using the ZSimpWin software from Princeton Applied Research (Oak Ridge, TN, USA). The effective capacitance C_s was extracted from the parameters of the constant phase element Q_s using the equation (2), as described in [13]:

$$C_s = \left[Q_s \left(R_s^{-1} + R_p^{-1} \right)^{\alpha_s - 1} \right]^{1/\alpha_s} \quad (2)$$

The effective capacitance C_f was approximated from the parameters of the constant phase element Q_f using equation (3), as described in [13]:

$$C_f = \sqrt[\alpha_f]{Q_f R_p}/R_p \quad (3)$$

The density of states at the Fermi level $D(E_F)$ was calculated using the equation (4), as detailed in [14]:

$$D(E_F) = C_{solid}^2/(\varepsilon \varepsilon_0 e) \quad (4)$$

where ε, ε_0, and e are the dielectric constant, vacuum permittivity, and the elementary charge of the electron, respectively. We assume an average dielectric constant of 3.23 characteristic for proteins [15].

2.7. Light microscopy

Fiber skeletons were examined after experiments using a Zeiss Axioplan 2 microscope. The length and width of the filaments were recorded using Image Pro Insight (Media Cybernetics). Images were acquired at different magnifications with an Exi Blue Camera (QImaging). Post-processing of the images was done using Fiji software.

2.8. Scanning electron microscopy (SEM)

Samples were prepared and washed as described above, and then placed using custom-made glass hooks on 1 × 1 cm diced Au-coated silicon wafers mounted on stainless steel discs with silver paste. Samples were left to dry overnight and imaged without any further

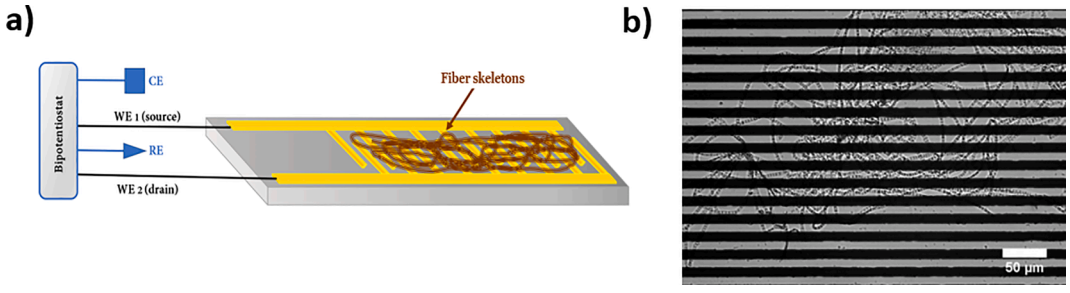

Fig. 2. a) Schematic of electrochemical gating measurement. WE1 and WE2 – working electrodes, CE – counter electrode, RE – reference electrode. b) Micrograph of a bundle of fiber skeletons deposited on the interdigitated gold electrode.

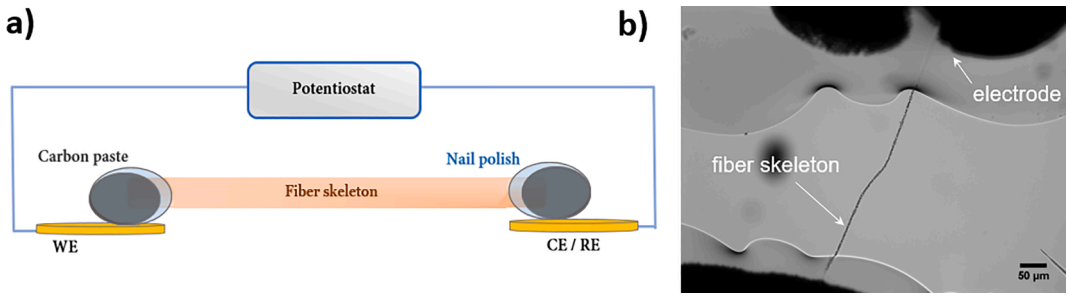

Fig. 3. a) Schematic of measurements of an individual fiber skeleton. WE – working electrode, CE – counter electrode, RE – reference electrode. b) Micrograph of an individual fiber skeleton stretched between electrical contacts (carbon pads waterproofed by nail polish).

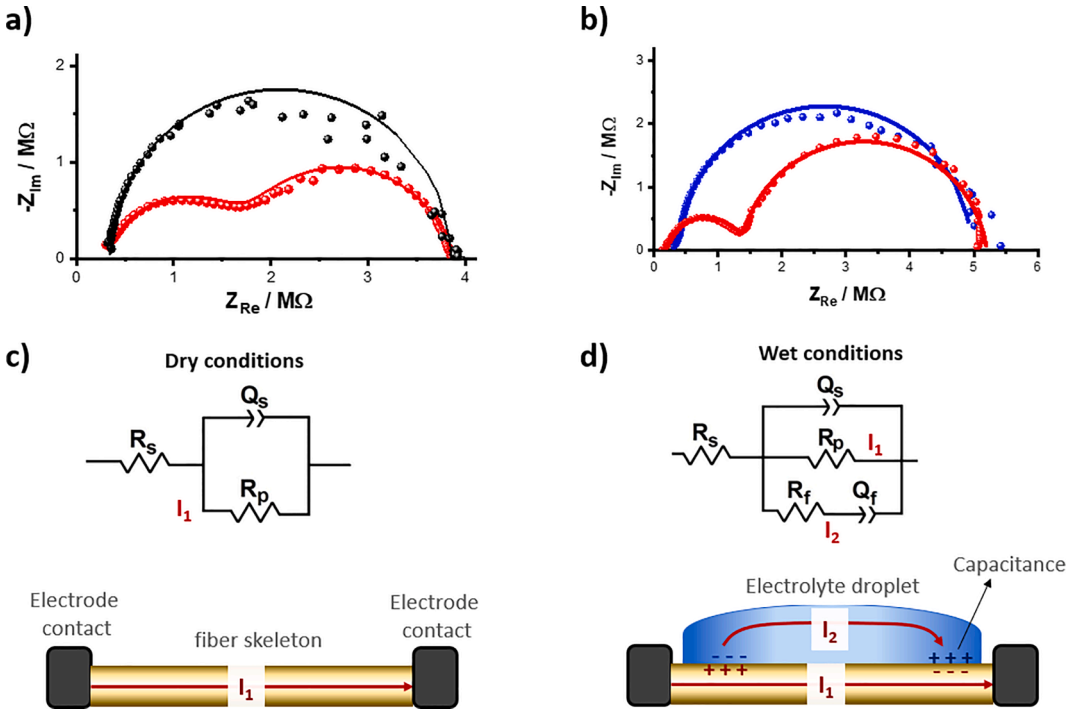

Fig. 4. Electrochemical impedance spectroscopy of a single cable bacterium fiber skeleton. Experimental data (dots), model fits (lines) and equivalent electrical circuits are shown. a) Representative Nyquist plots for the same single fiber skeleton shown for dry conditions (black) and wet conditions (submerged in phosphate buffer electrolyte; red). Fitting parameters are given in Table S2. b) Nyquist plots of an individual fiber skeleton submerged in deionized water (blue) and electrolyte solution (phosphate buffer; red). Fitting parameters are given in Table S3. c) and d) Equivalent electrical circuit models used in the fitting of the experimental data in dry/wet deionized (c) and wet electrolyte (d) conditions.

metallization. Imaging was performed on a Magellan 400L XHR Scanning Electron Microscope (FEI Company, USA) using secondary electron detector. Working distances, beam energies and tilt angles were optimized to improve image quality.

3. Results and discussion

3.1. High fiber conductivity in the dry state

To determine the electrical properties of the internal fiber network, native cable bacterium filaments were individually isolated from enrichment cultures. SEM micrographs of native filaments reveal the characteristic ridge pattern of the outer surface, as well as the cell–cell interface between individual cells (Fig. 1a). Each ridge compartment harbours a single conductive fiber that remains continuous across cell junctions and runs along the entire multicellular filament [5]. A sequential extraction procedure allows to remove the lipid membranes and cytoplasm from native filaments (Fig. 1c) [8], thus retaining a "fiber skeleton" that comprises the conductive fiber network connected by an underlying polysaccharide sheath [5,8]. These extracted fiber skeletons are flattened and wider than native filaments, and conspicuously, we noted that fibers showed up as bright lines in the EM images, running in parallel along the longitudinal axis of the fiber skeleton (Fig. 1b). This increased brightness reflects a higher emission yield of secondary electrons, thus suggesting a marked increase in the conductivity of the fibers compared to the surrounding material. The dimensions of the individual fibers (fiber diameter: 60 ± 6 nm) and the topology of the fiber network (center-to-center distance between parallel fibers: 172 ± 26 nm) are consistent with previous microscopic observations [8].

The macroscopic size of the fiber skeletons (~5 µm width, >2 mm length) enables them to be connected to metal electrodes for electrical characterization in the dry state [5] (setup in Fig. 3), thus avoiding the complexity and potential artifacts of nanoscopic investigations. Two-point current–voltage characterization of individual fiber skeletons in the dry state shows a highly linear current response over the applied voltage range of −0.2 to 0.2 V (Fig. S1 in Supporting Information). Based on the number of fibers per fiber skeleton, and the cross-sectional area of the fibers as determined by electron microscopy, the fiber conductivity

can be calculated (see Materials and Methods). The median conductivity (27 S cm^{-1}; N = 26) and observed range (2–564 S cm^{-1}; Table S1) align well with previous investigations on dry samples [5,10]. The variability between fiber skeletons is poorly understood but could result from damage incurred during isolation and extraction. The maximum fiber conductivity that we recorded was 564 S cm^{-1} (Fig. 1d, Table S1), which is on par with the highest conductivities recorded in synthetic organic polymers [16] and exceptionally high for a biological material [17]. This underscores the extraordinary character of the native conductive fiber network in cable bacteria. Conductance measurements of individual pili of *Geobacter sulfurreducens* provide conductivity values that are three orders of magnitude lower (0.03–0.05 S cm^{-1}), when wild-type pili are prepared and investigated similar as is done here (preparation at physiological pH with subsequent air drying, investigation via nanopatterned gold electrodes [18,19]). However, higher conductivity values are obtained when cytochrome OmcZ nanowires from *Geobacter sulfurreducens* are grown under an electric field (30 S cm^{-1} at pH 7) or when pili are prepared at lower pH (400 S cm^{-1} at pH 2) [20]. Future work should investigate whether fiber skeletons from cable bacteria exhibit a similar dependence on pH and electrical field.

3.2. Solvation and ionic strength have no impact on fiber conductivity

The above conductivity values are determined on dried samples, as was done in previous works where the conductance of cable bacteria was investigated [5,10]. *In vivo*, however, long-distance electron transport in cable bacteria takes place in an aqueous environment with high ionic strength, like freshwater [21] or marine sediments [7], and groundwater aquifers [22]. As in other Gram-negative bacteria, the periplasmic space in cable bacteria acts as an ionic medium with plenty of mobile ions [23]. As electrical fields can be sustained in the bulk of a solid, but not in an aqueous ionic medium, this has important repercussions for relating the experimental conductivity values to actual *in vivo* conduction and microbial physiology. Effectively, the rate of electron transport in biological protein structures has been shown to exhibit a strong dependence on the availability of water and ions [24]. For example, heme-heme electron transfer rates in the outer membrane decaheme cytochrome MtrF of *Shewanella* show a strong dependence on sample humidity, with dry samples providing a markedly higher conductance [25]. Following Marcus electron transport theory, the explanation is that increased solvent polarization and ionic screening induce higher reorganization energy, thus slowing down electron transfer [26].

Therefore, we expected a prominent effect of solvation and ionic strength on fiber conductivity in cable bacteria. To test this, we investigated individual fiber skeletons using alternating current electrochemical impedance spectroscopy (EIS) over a wide frequency range (see 2.4.2. in Materials and methods). EIS investigations were first done in the dry state (after fiber skeletons were air dried), followed by immersion of the same fiber skeleton in air-saturated deionized H_2O (wet non-ionic state) or air-saturated aqueous ionic buffer solution (wet ionic state). Our results are displayed in the form of Nyquist plots, which depict the imaginary part (Z_{Im}) versus the real part (Z_{Re}) of the impedance (Fig. 4, Table S2). When fiber skeletons were examined in the dry state (Fig. 4a), the Nyquist plots always displayed a single semicircle [10]. Remarkably, the same single semicircle response was observed when a drop of deionized water was deposited onto the fiber skeleton (Fig. 4b), thus indicating that solvation does not impact conductance.

When a drop of electrolyte was added, the EIS spectrum displays the same total resistance (i.e. the Z_{Re} value at low frequencies where the Nyquist curve intersects the x-axis), but shows an additional inflection point within the semicircle at intermediate frequencies (Fig. 4a,b; the origin of this inflection point is discussed below). A prominent observation is that these wet EIS spectra do not feature the hallmark of an ionic diffusion process at low frequencies, i.e., a curved tail followed by a linear increase of Z_{Im} with Z_{Re}. The emergence of such a diffusive tail would be expected, as it reflects the effect of counterion transport on conduction, as for example, seen in EIS measurements on protein biofilms amended with heme groups [27]. While the absence of ionic diffusion can be explained in the dry state, as ions could become immobile during drying, it is remarkable that the diffusive low-frequency response is not observed in the wet ionic state representative of *in vivo* conditions. Overall, the fiber skeletons do not show any impacts of solvent polarization and ionic screening on electron transport, which appreciably contrasts with what is normally seen in other conductive protein structures, such as multiheme cytochromes [25,28].

3.3. The electrical circuitry inside cable bacteria

To further constrain the electrical properties of the fiber network, we fitted the EIS data to equivalent electrical circuits (EEC) featuring resistors (R), capacitors (C) and constant phase elements (Q) that represent non-ideal capacitances (Fig. 4c,d). The comparison of EIS spectra between fiber skeletons of different lengths (N = 9, Table S2) allows for a physical interpretation of the different components. The EEC that fits the experimental data best in the dry (and also non-ionic wet state) state includes a resistance R_s in series with a constant phase element Q_s and a second resistance R_p (Fig. 4c). A similar EIS behaviour was recorded for a conductive line of CNTs (Fig. S3), which confirms that the presence of R_s and Q_s in the EEC is not related to the sample (fiber skeletons or CNTs), but can be directly linked to the experimental set-up.

R_s was consistently low (0.26 ± 0.04 MΩ) across all samples, remained invariant between different fiber skeletons, and did not depend on the presence of the buffer solution (no difference between wet and dry conditions). We interpret R_s as the combined resistance of the external circuit and the contact resistance at the interface between the fiber skeleton and electrode. Likewise, the effective capacitance C_s (as calculated from the constant phase element Q_s) was small (C_s = 3.4 ± 0.3 pF) and did not correlate with the length or conductivity of the fiber skeletons investigated. C_s likely represents a small parasitic capacitance of the experimental setup combined with a non-ideal capacitance at the interface between the fiber skeleton and electrodes. The resistance R_p can be interpreted as the intrinsic resistance of the conductive fiber network in the cable bacterium filaments. Intriguingly, this implies that the fiber network exclusively acts as an ohmic conductor and does not display any capacitance.

The EIS spectra in the wet electrolyte state display an inflection point within the semicircle. This feature can be explained by an EEC that includes an additional current loop with a resistance R_f in series with a capacitance C_f, representing current through the new interface between the fiber skeletons and the surrounding ionic buffer (Fig. 4d). To experimentally test this EEC, we added a third electrical contact point in the middle of the fiber skeleton (Fig. S2). The EIS spectra for various terminal end configurations (1–3, 1–2 and 2–3 connections) fully support the proposed EEC (Fig. S2 and Additional Results in SI). Furthermore, a model sensitivity analysis of the EEC consistently reproduces the transition from the one semi-circle behaviour in the “dry” state of Fig. 4c to the two-semi-circle behaviour in the “wet ionic” state of Fig. 4d (Fig. S4 and Additional Results in SI).

Comparison between dry and wet states also provides insight into the topology of the current network. In the dry state, there is only one current pathway (I_1) that runs between the electrode contacts, and hence all the current goes through the conductive fibers (Fig. 4c). In contrast, in the wet electrolyte state, there are two parallel current pathways: the I_1 current (running through the conductive fiber) and the I_2 current, the physical nature of which is not entirely clear and requires additional investigation. The resistance of the electrolyte-related pathway (R_f = 0.6–4.0 MΩ) and its additional capacitance C_f (8–180 pF, i.e. 0.3–5.0 μF cm^{-2}) suggests there is an accumulation of charge at the interface between the fiber skeleton and ionic solution via the formation of a double layer (Fig. 4d). The corresponding capacitance density (0.3–5.0 μF cm^{-2}) resembles that of metal surfaces (e.g. gold [29] and copper [30]) with an adsorbed monolayer of thiols (thickness

< 6 nm) or pyrolytic graphite modified with a layer of nitrocellulose [31,32]. Using an average dielectric constant for protein ($\varepsilon = 3.23$) [15], and accounting for the surface area of the fiber skeleton exposed to the electrolyte solution ($A = 2.5{\cdot}10^{-5}$ cm^2 for the sample 4, Table S2), we estimate that the conductive structures must be covered with an insulating layer of maximal thickness ~ 9.5 nm, which aligns well with the recent proposition that the fibers contain a highly conductive core surrounded by a non-conductive shell, as recently derived from by electrostatic force imaging [4].

Remarkably, in all our experiments, the resistance of the fiber current pathway (R_p) is always the same in the dry and wet electrolyte states. In the dry state, R_p varied from 2.2 to 8.1 MΩ between filaments (Table S2), and accounting for the length of the fiber skeleton, these R_p values translate into a fiber conductivity in the range of 11–35 S cm^{-1}, consistent with the values obtained from our DC measurements (Fig. 1d). When a drop of the electrolyte solution is added on top of the fiber skeletons, the R_p values remain invariant (Fig. 5a). This confirms that the fiber network retains its high conductivity in electrolyte conditions representative of *in vivo* (50 mM phosphate buffer containing 0.1 M KCl, pH 7).

3.4. Temperature dependence of fiber conduction in aqueous conditions

Conductivity probing as a function of temperature provides insight into the underlying electron transport mechanism. However, it is challenging to use single filaments for such measurements, due to the specific design of the experimental setup and the associated sensitivity of the current signal readout. To attain a higher current signal, multiple fiber skeletons ("bundles") were deposited on interdigitated gold electrodes (IGEs) and temperature-dependent EIS measurements were conducted in a buffer solution (wet ionic state, mimicking *in vivo* conditions). The conductance increases with temperature over the relevant physiological range (0–30 °C), thus indicating that electron transport in the periplasmic fibers is a thermally activated process. A linear fit of the data to the Arrhenius equation (Fig. 5b) yields activation energy ($E_a = 69 \pm 23$ meV), which is close to the value for dry single fiber skeletons measured in vacuum (42 ± 23 meV [33]) or under N_2 atmosphere (49 ± 7 meV [10]). This result has two important ramifications. Foremost, the immersion in an electrolyte solution does not appear to change the reorganization energy (λ) of the electron transport. Secondly, the reorganization energy ($\lambda = 4E_a = 0.2$–0.3 eV) is remarkably low compared to other forms of biological conduction. For example, charge transport in multi-heme cytochromes and other metalloproteins is typically characterized by a reorganization energy λ of 0.7–1.2 eV [34,35], while electron transport in the surface appendages of metal-reducing bacteria also shows a 4–6 fold higher thermal activation ($\lambda \sim 1.2$ eV [36]).

3.5. Electrochemical gating reveals lack of redox signature

The conventional notion of long-range electron transport through microbial systems is centrally based on the concept of redox conduction [37,38], in which the conductor consists of a chain of connected redox molecules, and electrons are transferred via self-exchange reactions between adjacent redox centers coupled to the motion of counter-balancing ions to maintain electroneutrality [39,40]. However, cyclic voltammetry in an electrolyte solution under anoxic conditions does not reveal any redox response of the fiber skeletons (Fig. S5). The distinctive rectangular shape of the cyclic voltammogram indicates a typical capacitive behaviour and the absence of redox transformation of any surface-confined species. Strikingly, the fiber skeletons do not show any sign of redox activity, which is congruent with the absence of any intrinsic capacitance associated with the fibers in the EEC.

To further assess whether the conduction mechanism is redox-mediated or not, we applied the electrochemical gating technique [38]. By changing the potential of the electrode, one measures the conductance as a function of the oxidation state of the redox moieties embedded in the conductor. The source and drain potentials (E_S and E_D) are controlled by a bipotentiostat and scanned simultaneously at the same rate ν, while maintaining a constant small source-drain voltage ($V_{SD} = E_D - E_S$). Electrochemical gating of electrogenic biofilms [41–43] shows a characteristic peak-shaped dependence, where the gate potential at maximum conductance corresponds to the formal potential of cytochromes [36,41] and other cofactors [44] that act as reducible/oxidisable charge carriers [38,43]. Hence, the question is whether long-range conduction in cable bacteria also exhibits a similar redox signature.

To test this, we applied electrochemical gating to fiber skeletons deposited onto interdigitated gold microelectrode arrays (Fig. 2) submerged in air-saturated aqueous electrolyte solutions (see 2.3 and 2.4.1 in Materials and methods). To verify our experimental procedure, three reference materials were also evaluated under identical experimental conditions. When the soluble redox mediator $[Ru(NH_3)_6]^{3+}$ was added to the solution, the source-drain current showed the expected bell-shaped dependency on the gate potential (Fig. 6a), and the maximum current was observed at −0.19 V vs. SCE, which coincides with the

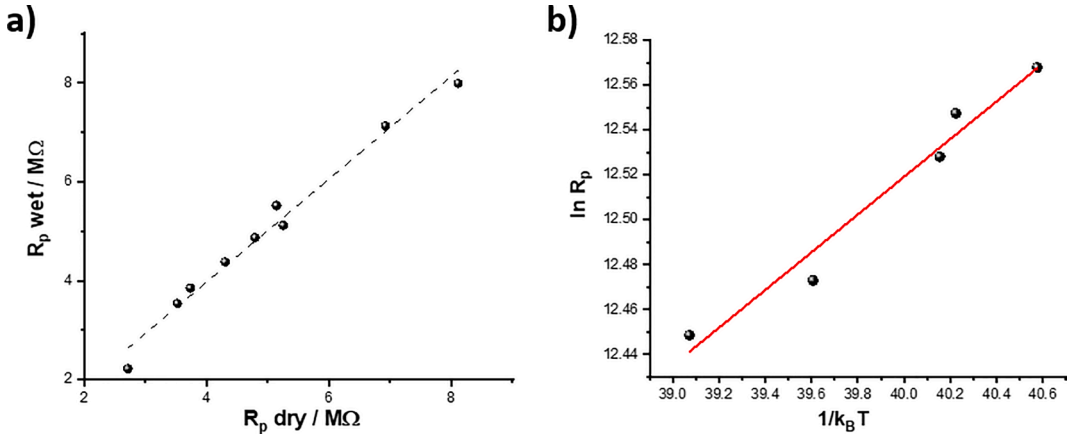

Fig. 5. Fiber skeletons display the same electrical properties in dry and wet electrolyte conditions. a) The resistance (R_p) dry state versus immersed in electrolyte solution (R_p values as obtained from fitting the equivalent electrical models in Fig. 2). Dashed line represents 1:1 line. A switch from dry to wet conditions has no impact on the conductance of the fiber skeleton. b) Temperature dependence of the resistance R_p of fiber skeletons in the wet ionic state over the range from 0 to 30 °C. The data for one representative IGE sample is shown. The solid red line is the Arrhenius fit. The activation energy $E_a = 69 \pm 23$ meV was determined from n = 3 three independent IGE replicates.

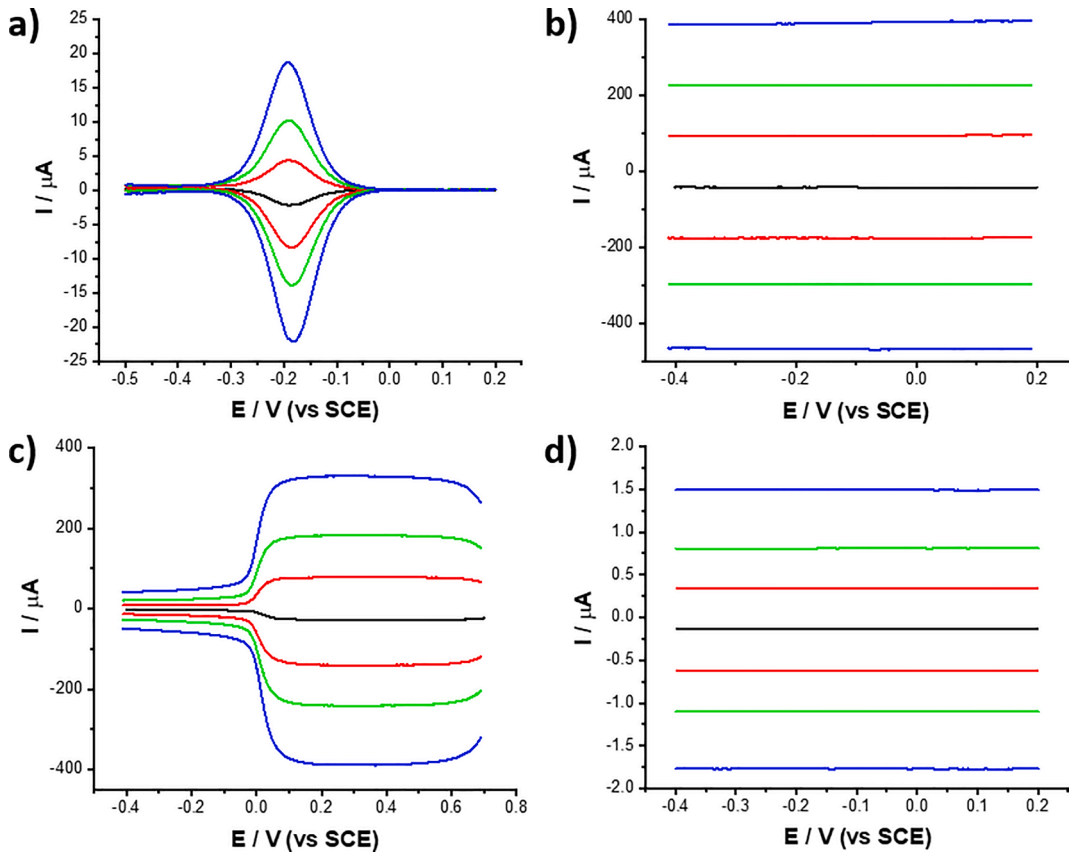

Fig. 6. Electrochemical gating measurements. Dependence of source-drain current I on the source electrode potential E for 1 mM $[Ru(NH_3)_6]^{3+}$ in 0.1 M KCl (a), CNTs in phosphate buffer, pH 7 (b), PANI/CNT composite in 0.5 M H_2SO_4 (c), fiber skeletons of cable bacteria in phosphate buffer, pH 7 (d). Source-drain voltage: 0 mV (black curves), 3 mV (red curves), 6 mV (green curves), and 10 mV (blue curves). Scan rate: 5 mV s^{-1}. Background current output was recorded from bare mercaptohexanol-modified interdigitated gold electrodes under the same conditions and subtracted from the curves presented.

known value for the redox potential of $[Ru(NH_3)_6]^{3+/2+}$ [45]. This bell-shaped response is characteristic for redox-mediated electron transport, as an electrical current can only pass when the redox compound is neither fully reduced nor fully oxidized. In contrast, we observed a very different gating response when carbon nanotubes (CNTs) were dropcast on the surface of IGE. These CNTs act as a classical ohmic conductor and do not show any redox dependence. The gating current remained independent of the gate potential, while the magnitude of the observed gating current linearly scales with the applied source-drain voltage (Fig. 6b). As a third reference material, we investigated a composite film of polyaniline (PANI) and multi-walled CNTs, which showed a mixture of redox-mediated and redox-independent behaviour (Fig. 6c). The gating current remained constant for negative potentials, but then strongly increased when PANI underwent redox transformations between fully reduced (leucoemeraldine) and partially oxidized (emeraldine) forms [11,46] respectively near 0 V vs. SCE. These three materials provide a reference frame for the electrochemical gating response of the fiber skeletons, which turned out to be highly similar to that of CNTs. The gating current remained independent of the gating potential throughout the whole potential window (Fig. 6d). This indicates that redox active species are not involved in appreciable amounts in the electron transport process, thus corroborating the findings of our voltammetric measurements.

The "flat" gating response (Fig. 6d) provides critical insight into the charge-carrier concentration in the fiber network. During electrochemical gating experiments, the fiber network acts as a solid-phase electron conductor that is brought into contact with an ionic solution. The polarization of the gate electrode causes the formation of an electrical double layer at the interface between the electrolyte solution and the conductive filament. This interface has a capacitance C_f as demonstrated by our EIS experiments (C_f emerges when adding a drop of electrolyte – see Fig. 4d). The overall capacitance is located partly at the solid side and partly at the solution side, and can be described by a series connection of two capacitors C_{solid} and C_{DL}, respectively ($1/C_f = 1/C_{solid} + 1/C_{DL}$) [47].

Depending on the charge-carrier concentration in the solid (which determines C_{solid}), two endmember situations arise. If the filament acts as an intrinsic semiconductor, then the charge-carrier concentration and capacitance are typically low ($C_{solid} \ll C_{DL}$). As a result, a relatively wide interphase region will form within the solid (~100 nm), which is enriched with charge carriers (electrons or holes, depending on the polarization of the gate electrode). Upon increasing the gate potential, the Fermi level in the interfacial layer will change with respect to the conduction band edge, and in this way, the charge carrier concentration in the interfacial layer is strongly increased. As a result, electrochemical polarization will strongly modulate the conductance of the semiconductor, and hence a strong gating response is expected. Conversely, if the filament would act as a metal, then the charge-carrier concentration and capacitance are high ($C_{solid} \gg C_{DL}$). A change of the gate potential then mainly leads to a change in the potential drop across the electrochemical double layer, and the charge-carrier concentration in the solid remains essentially unchanged. In this case, no gating response is expected.

The absence of a gating response (Fig. 6d) suggests that the fiber network acts far more metal-like than semiconductor-like. Using a typical differential capacitance for the Helmholtz layer (C_{DL} = 18 µF cm^{-2}), and using our EIS-based estimates for C_f while accounting for the average surface area of the fiber skeletons in contact with the electrolyte solution ($A = 2 \times 10^{-9}$ m^2), we can estimate $C_{solid} = (1/C_f - 1/C_{DL})^{-1}$ as 0.3–6.9 µF cm^{-2}. Accordingly, the C_{solid} capacitance of the fibers

skeletons is high, matching that of CNTs [48]. The density of states at the Fermi level obtained from these C_{solid} values is in the range of 2.0×10^{18}–1.0×10^{21} cm^{-3} eV^{-1}, which is close to that for CNTs [49]. This corroborates the idea that the conductive fibers must have a high charge carrier concentration for an organic biological material.

3.6. Unconventional biological charge transport in cable bacteria

In this work, we have performed a detailed electrical and electrochemical characterization of fiber skeletons from cable bacteria, which are obtained by sequential extraction, thus selectively removing membranes and cytoplasm, while retaining the periplasmic fiber network connected by a carbohydrate sheath. Previous work has shown that this extraction procedure does not appear to structurally or functionally affect the conductive fiber network. There is no difference in the shape of the *I/V* curves, and also the resulting fiber conductivities remain similarly high, before and after extraction [5]. In this work, the charge transport in cable bacteria was investigated in the presence of electrolyte solution, which approaches more closely the physiological conditions of *in vivo* operation compared to earlier results on air-dried filaments or measurements obtained in vacuum. Remarkably, we find no major differences between wet and dry conditions. The fiber network retains a similar high conductivity as well as a similar activation energy in electrolyte solution compared to dry conditions (Fig. 5). Foremost, this implies that previous electrical characterization in vacuum or under N_2 atmosphere seems to be relevant for the *in vivo* operation of the network. More importantly, it is highly remarkable that a protein structure retains its function upon desiccation, as drying can significantly affect the functional properties of proteins [50]. This hence suggests that the fiber network has a robust architecture that is resistant to conformational changes.

Currently, the default model for long-distance biological electron transport is redox conduction, which assumes sequential short-distance electron transfer reactions (“small polaron hopping”) between adjacent redox cofactors [38,51]. Importantly, redox conduction occurs within an ionic medium, where ionic screening counteracts the build–up of any electrical field. As a consequence, redox conduction is essentially “concentration driven”: it requires a gradient in the concentration of reduced redox sites to drive the electron exchange along the current direction. The absence of any peaks in the gating response (Fig. 6) however demonstrates that fiber conduction in cable bacteria is not based on redox conduction, and hence field-driven rather than concentration-driven [52].

In addition to the non-redox nature, there are other aspects in which conduction in cable bacteria differs from the known forms of biological long-range electron transport. Foremost, the fiber conductivity remains invariant upon the presence of water (Fig. 4a) and ions (Fig. 4; Table S2, Fig. 5a), while thermal activation is also similar under dry and wet conditions (Fig. 5b). The absence of any ionic screening effects corroborates the idea that the electron transport inside the fibers is field-driven in both dry and wet conditions and is also consistent with the core–shell model proposed by Boschker et al. [4], in which the conductive core is surrounded by an outer nonconductive shell that restricts the mobility of ions.

Furthermore, our data suggest the fibers have a high free charge carrier density (Fig. 6), while the reorganization energy is substantially lower compared to electron transport in other metalloprotein systems (Fig. 5b). Due to the combination of high conductivity, high charge carrier density, and low activation energy, the conduction mechanism resembles that of a “molecular semi-metal”, i.e., a non-metallic organic material whose properties resemble those of metals [53]. In organic semiconductors, low activation energies are associated with low static dielectric constants, sizeable conjugation and the creation of polarons in which electrons are delocalized across multiple charge carrier sites [54]. We hypothesize that a similar “delocalized polaron” mechanism could be active in the conductive fibers of cable bacteria.

4. Conclusions

Our findings provide a more detailed insight into the electron transfer phenomenon that enables metabolic currents across centimeter distances. Detailed electrochemical characterization of protein fibers of cable bacteria indicates that these microorganisms have evolved a form of biological conduction to transport electrons over long distances. The conduction mechanism displays a unique combination of features, including an exceptionally high conductivity (up to 565 S cm^{-1}), a low reorganization energy (λ = 0.2–0.3 eV), a high density of states at the Fermi level (2.0×10^{18}-1.0×10^{21} cm^{-3} eV^{-1}), the absence of a redox signature, and no effect of wetting or the presence of electrolytes on the conductivity. Together, these features indicate that the conduction mechanism in the conductive fibers of cable bacteria does not fit the Marcus model (i.e., small polaron hopping), which is conventionally invoked to explain electron transfer in metalloproteins.

The electrical measurements performed here require that the fiber skeletons structures make contact with gold-patterned electrodes. One remarkable finding is that the fibers skeletons make an easy electric contact with the gold pads. While our data show there is a contact resistance, there is efficient charge injection into the fiber network that conveys the current along the filament. It has been previously hypothesized that the fibers consist of a conductive core surrounded by an insulating layer [4]. Hence the problem arises of how to upload and download electrons onto the fiber network. In living bacteria, it has been speculated that periplasmic cytochromes serve this role, acting as electron shuttles that can connect to fibers. However, in fiber skeletons, cytochromes are removed during extraction [5], and so the question remains how electrons can efficiently move from the gold electrode to and from the fiber network. More detailed insight into the structure of the fiber skeletons is required to shed light on this issue.

In a similar way, the charge transport through the fiber network remains equally enigmatic. Recently, it has been shown that the conductive fibers of cable bacteria contain a sulfur ligated Ni-group, which possesses a configuration that is different from all other known prosthetic groups involved in biological electron transport (which are either Fe- or Cu- based) [4,33]. Polaron delocalization across multiple Ni-S cofactors could explain the low reorganization energy and semi-metallic properties observed [33,55]. However, to verify this hypothesis, a better understanding into the molecular structure of this Ni-S cofactor is necessary, and a more detailed insight into the arrangement of the Ni-S cofactors in the fiber structure is required.

Data availability

The conductance data supporting the histogram in Fig. 1d are provided in Table S1. The data supporting the EIS results are provided in Tables S2-S6. Other data supporting the findings of this study are available from the corresponding author upon reasonable request.

The ZSimpWin scripts that were used in the fitting of the equivalent electrical circuits (Fig. S4) are available from the corresponding author upon request.

CRediT authorship contribution statement

Dmitrii Pankratov: Writing – review & editing, Writing – original draft, Visualization, Validation, Methodology, Investigation, Formal analysis, Data curation. **Silvia Hidalgo Martinez:** Methodology, Investigation. **Cheryl Karman:** Methodology, Investigation, Formal analysis, Data curation. **Anastasia Gerzhik:** Visualization, Methodology, Investigation. **Gabriel Gomila:** Software, Methodology, Investigation, Formal analysis. **Stanislav Trashin:** Methodology, Investigation. **Henricus T.S. Boschker:** Methodology, Investigation, Formal analysis. **Jeanine S. Geelhoed:** Methodology, Formal analysis. **Dirk Mayer:** Visualization, Methodology, Investigation, Conceptualization. **Karolien De Wael:** Supervision, Methodology, Funding acquisition, Conceptualization. **Filip J.R. Meysman:** Writing – review & editing, Writing – original draft, Visualization, Validation, Supervision,

Resources, Project administration, Methodology, Funding acquisition, Formal analysis, Data curation, Conceptualization.

Declaration of competing interest

The authors declare that they have no known competing financial interests or personal relationships that could have appeared to influence the work reported in this paper.

Data availability

Majority of data are included in the manuscript. Other data supporting the findings of this study are available from the corresponding author upon reasonable request.

Acknowledgements

The authors thank Elke Brauweiler-Reuters for support during recording the SEM images.

HTSB and FJRM were financially supported by the Netherlands Organization for Scientific Research (VICI grant 016.VICI.170.072). Research Foundation Flanders supported DP, CK, KDW, and FJRM through FWO grant G043119N. ST, KDW and FJRM received support by University of Antwerp via the TopBOF program. DM, GG, JSG, SHM, and FJRM received support from the EIC (Pathfinder project 101046719 PRINGLE).

Author contributions

FJRM and KDW designed the study. FJRM coordinated data collection and analysis. SHM and JSG performed filament cultivation and fiber skeleton extraction. AG, SHM, and DM performed SEM image collection. HTSB, DP and SHM performed electrical characterization via *I/V* curves of single filaments. CK, ST, DP and SHM conducted electrochemical gating experiments. DP and SHM conducted EIS measurements, while DP and FJRM analyzed the results and developed the electrical equivalent models. GG and FJRM conducted modelling of electrical equivalent circuits. DP determined the temperature dependence of filament conductance. DP and FJRM wrote the paper with contributions provided by all co-authors.

Appendix A. Supplementary data

Supplementary data to this article can be found online at https://doi.org/10.1016/j.bioelechem.2024.108675.

References

[1] H.B. Gray, J.R. Winkler, Electron flow through metalloproteins, BBA-Bioenergetics 1797 (2010) 1563–1572.
[2] C. Pfeffer, S. Larsen, J. Song, M.D. Dong, F. Besenbacher, R.L. Meyer, K.U. Kjeldsen, L. Schreiber, Y.A. Gorby, M.Y. El-Naggar, K.M. Leung, A. Schramm, N. Risgaard-Petersen, L.P. Nielsen, Filamentous bacteria transport electrons over centimetre distances, Nature 491 (2012) 218–221.
[3] F.J.R. Meysman, Cable bacteria take a new breath using long-distance electricity, Trends Microbiol. 26 (2018) 411–422.
[4] H.T.S. Boschker, P.L.M. Cook, L. Polerecky, R.T. Eachambadi, H. Lozano, S. Hidalgo Martinez, D. Khalenkow, V. Spampinato, N. Claes, P. Kundu, D. Wang, S. Bals, K.K. Sand, F. Cavezza, T. Hauffman, J.T. Bjerg, A.G. Skirtach, K. Kochan, M. McKee, B. Wood, D. Bedolla, A. Gianoncelli, N.M.J. Geerlings, N. Van Gerven, H. Remaut, J.S. Geelhoed, R. Millan-Solsona, L. Fumagalli, L.P. Nielsen, A. Franquet, J.V. Manca, G. Gomila, F.J.R. Meysman, Efficient long-range conduction in cable bacteria through nickel protein wires, nature, Communications 12 (2021) 3996.
[5] F.J.R. Meysman, R. Cornelissen, S. Trashin, R. Bonne, S. Hidalgo Martinez, J. van der Veen, C.J. Blom, C. Karman, J.L. Hou, R.T. Eachambadi, J.S. Geelhoed, K. De Wael, H.J.E. Beaumont, B. Cleuren, R. Valcke, H.S.J. van der Zant, H.T.S. Boschker, J.V. Manca, A highly conductive fibre network enables centimetre-scale electron transport in multicellular cable bacteria, nature, Communications 10 (2019) 4120.
[6] L.P. Nielsen, N. Risgaard-Petersen, H. Fossing, P.B. Christensen, M. Sayama, Electric currents couple spatially separated biogeochemical processes in marine sediment, Nature 463 (2010) 1071–1074.
[7] S.Y. Malkin, A.M.F. Rao, D. Seitaj, D. Vasquez-Cardenas, E.M. Zetsche, S. Hidalgo Martinez, H.T.S. Boschker, F.J.R. Meysman, Natural occurrence of microbial Sulphur oxidation by long-range electron transport in the seafloor, ISME J. 8 (2014) 1843–1854.
[8] R. Cornelissen, A. Boggild, R.T. Eachambadi, R.I. Koning, A. Kremer, S. Hidalgo Martinez, E.M. Zetsche, L.R. Damgaard, R. Bonne, J. Drijkoningen, J.S. Geelhoed, T. Boesen, H.T.S. Boschker, R. Valcke, L.P. Nielsen, J. D'Haen, J.V. Manca, F.J. R. Meysman, The cell envelope structure of cable bacteria, Front. Microbiol. 9 (2018) 3044.
[9] R.T. Eachambadi, R. Bonne, R. Cornelissen, S. Hidalgo Martinez, J. Vangronsveld, F.J.R. Meysman, R. Valcke, B. Cleuren, J.V. Manca, An ordered and fail-safe electrical network in cable bacteria, advanced, Biosystems 4 (2020) 2000006.
[10] R. Bonne, J.L. Hou, J. Hustings, K. Wouters, M. Meert, S. Hidalgo-Martinez, R. Cornelissen, F. Morini, S. Thijs, J. Vangronsveld, R. Valcke, B. Cleuren, F.J. R. Meysman, J.V. Manca, Intrinsic electrical properties of cable bacteria reveal an arrhenius temperature dependence, Sci. Rep. 10 (2020) 19798.
[11] G. Otrokhov, D. Pankratov, G. Shumakovich, M. Khlupova, Y. Zeifman, I. Vasil'eva, O. Morozova, A. Yaropolov, Enzymatic synthesis of polyaniline/multi-walled carbon nanotube composite with core shell structure and its electrochemical characterization for supercapacitor application, Electrochim. Acta 123 (2014) 151–157.
[12] F.J.R. Meysman, N. Risgaard-Petersen, S.Y. Malkin, L.P. Nielsen, The geochemical fingerprint of microbial long-distance electron transport in the seafloor, Geochim. Cosmochim. Acta 152 (2015) 122–142.
[13] M.E. Orazem, B. Tribollet, Electrochemical impedance spectroscopy, John Wiley & Sons Inc, 2008.
[14] H. Gerischer, An interpretation of the double-layer capacity of graphite-electrodes in relation to the density of states at the Fermi level, J. Phys. Chem. 89 (1985) 4249–4251.
[15] M. Amin, J. Kuepper, Variations in proteins dielectric constants, Chemistry Open 9 (2020) 691–694.
[16] G. Prunet, F. Pawula, G. Fleury, E. Cloutet, A.J. Robinson, G. Hadziioannou, A. Pakdel, A review on conductive polymers and their hybrids for flexible and wearable thermoelectric applications, Materials Today Physics 18 (2021) 100402.
[17] J.T. Atkinson, M.S. Chavez, C.M. Niman, M.Y. El-Naggar, Living electronics: a catalogue of engineered living electronic components, microb, Biotechnol 16 (2023) 507–533.
[18] R.Y. Adhikari, N.S. Malvankar, M.T. Tuominen, D.R. Lovley, Conductivity of individual geobacter pili, RSC Adv. 6 (2016) 8354–8357.
[19] F. Wang, Y. Gu, J.P. O'Brien, S.M. Yi, S.E. Yalcin, V. Srikanth, C. Shen, D. Vu, N. L. Ing, A.I. Hochbaum, E.H. Egelman, N.S. Malvankar, Structure of microbial nanowires reveals stacked hemes that transport electrons over micrometers, Cell 177 (2019) 361–369.
[20] S.E. Yalcin, J.P. O'Brien, Y.Q. Gu, K. Reiss, S.M. Yi, R. Jain, V. Srikanth, P.J. Dahl, W. Huynh, D. Vu, A. Acharya, S. Chaudhuri, T. Varga, V.S. Batista, N.S. Malvankar, Electric field stimulates production of highly conductive microbial OmcZ nanowires, Nat Chem Biol 16 (2020) 1136–1142.
[21] N. Risgaard-Petersen, M. Kristiansen, R.B. Frederiksen, A.L. Dittmer, J.T. Bjerg, D. Trojan, L. Schreiber, L.R. Damgaard, A. Schramm, L.P. Nielsen, Cable bacteria in freshwater sediments, Appl. Environ. Microbiol. 81 (2015) 6003–6011.
[22] H. Müller, J. Bosch, C. Griebler, L.R. Damgaard, L.P. Nielsen, T. Lueders, R. U. Meckenstock, Long-distance electron transfer by cable bacteria in aquifer sediments, ISME J. 10 (2016) 2010–2019.
[23] K.U. Kjeldsen, L. Schreiber, C.A. Thorup, T. Boesen, J.T. Bjerg, T.T. Yang, M. S. Dueholm, S. Larsen, N. Risgaard-Petersen, M. Nierychlo, M. Schmid, A. Boggild, J. van de Vossenberg, J.S. Geelhoed, F.J.R. Meysman, M. Wagner, P.H. Nielsen, L. P. Nielsen, A. Schramm, On the evolution and physiology of cable bacteria, PNAS 116 (2019) 19116–19125.
[24] A. Lagunas, A. Guerra-Castellano, A. Nin-Hill, I. Diaz-Moreno, M.A. De la Rosa, J. Samitier, C. Rovira, P. Gorostiza, Long distance electron transfer through the aqueous solution between redox partner proteins, Nat. Commun. 9 (2018) 5157.
[25] H.S. Byun, S. Pirbadian, A. Nakano, L. Shi, M.Y. El-Naggar, Kinetic Monte Carlo simulations and molecular conductance measurements of the bacterial decaheme cytochrome MtrF, ChemElectroChem 1 (2014) 1932–1939.
[26] R.A. Marcus, N. Sutin, Electron transfers in chemistry and biology, BBA 811 (1985) 265–322.
[27] Y. Agam, R. Nandi, A. Kaushansky, U. Peskin, N. Amdursky, The porphyrin ring rather than the metal ion dictates long-range electron transport across proteins suggesting coherence-assisted mechanism, PNAS 117 (2020) 32260–32266.
[28] J. Blumberger, Electron transfer and transport through multi-heme proteins: recent progress and future directions, Curr. Opin. Chem. Biol. 47 (2018) 24–31.
[29] J.A.M. Sondag-Huethorst, L.G.J. Fokkink, Electrical double-layers on thiol-modified polycrystalline gold electrodes, J. Electroanal. Chem. 367 (1994) 49–57.
[30] G.K. Jennings, T.H. Yong, J.C. Munro, P.E. Laibinis, Structural effects on the barrier properties of self-assembled monolayers formed from long-chain omega-alkoxy-n-alkanethiols on copper, J. Am. Chem. Soc. 125 (2003) 2950–2957.
[31] D. Fapyane, E.E. Ferapontova, Electrochemical assay for a total cellulase activity with improved sensitivity, Anal. Chem. 89 (2017) 3959–3965.
[32] D. Pankratov, M. Bendixen, S. Shipovskov, U. Gosewinkel, E.E. Ferapontova, Cellulase-linked immunomagnetic microbial assay on electrodes: specific and sensitive detection of a single bacterial cell, Anal. Chem. 92 (2020) 12451–12459.
[33] J.R. van der Veen, S. Hidalgo Martinez, A. Wieland, M. de Pellegrin, R. Verweij, Y. M. Blanter, H.S.J. van der Zant, F.J.R. Meysman, Quantum-assisted electron

transport in microbial protein wires across macroscopic distances, Preprint at https://arxiv.org/abs/2308.09560, 2023.
[34] O.V. Kontkanen, D. Biriukov, Z. Futera, Reorganization free energy of copper proteins in solution, in vacuum, and on metal surfaces, J. Chem. Phys. 156 (2022) 175101.
[35] J. Liu, S. Chakraborty, P. Hosseinzadeh, Y. Yu, S.L. Tian, I. Petrik, A. Bhagi, Y. Lu, Metalloproteins containing cytochrome, iron-sulfur, or copper redox centers, Chem. Rev. 114 (2014) 4366–4469.
[36] S. Xu, A. Barrozo, L.M. Tender, A.I. Krylov, M.Y. El-Naggar, Multiheme cytochrome mediated redox conduction through *shewanella oneidensis* MR-1 cells, J. Am. Chem. Soc. 140 (2018) 10085–10089.
[37] S.M. Strycharz-Glaven, R.M. Snider, A. Guiseppi-Elie, L.M. Tender, On the electrical conductivity of microbial nanowires and biofilms, Energ. Environ. Sci. 4 (2011) 4366–4379.
[38] D.A. Boyd, R.M. Snider, J.S. Erickson, J.N. Roy, S.M. Strycharz-Glaven, L. M. Tender, Theory of redox conduction and the measurement of electron transport rates through electrochemically active biofilms, Biofilms in Bioelectrochemical Systems (2015) 177–210.
[39] N.F. Polizzi, S.S. Skourtis, D.N. Beratan, Physical constraints on charge transport through bacterial nanowires, Faraday Discuss. 155 (2012) 43–62.
[40] S. Pirbadian, M.Y. El-Naggar, Multistep hopping and extracellular charge transfer in microbial redox chains, PCCP 14 (2012) 13802–13808.
[41] M.D. Yates, J.P. Golden, J. Roy, S.M. Strycharz-Glaven, S. Tsoi, J.S. Erickson, M. Y. El-Naggar, S.C. Barton, L.M. Tender, Thermally activated long range electron transport in living biofilms, PCCP 17 (2015) 32564–32570.
[42] P.P. Liu, A. Mohamed, P. Liang, H. Beyenal, Effect of electrode spacing on electron transfer and conductivity of *geobacter sulfurreducens* biofilms, Bioelectrochemistry 131 (2020) 107395.
[43] M.D. Yates, S.B. Engel, B.J. Eddie, N. Lebedev, A.P. Malanoski, L.M. Tender, Redox-gradient driven electron transport in a mixed community anodic biofilm, FEMS Microbiol. Ecol. 94 (2018) fiy081.
[44] M.D. Yates, B.J. Eddie, N.J. Kotloski, N. Lebedev, A.P. Malanoski, B.C. Lin, S. M. Strycharz-Glaven, L.M. Tender, Toward understanding long-distance extracellular electron transport in an electroautotrophic microbial community, Energ. Environ. Sci. 9 (2016) 3544–3558.
[45] G. Pankratova, J.Y. Pan, S.S. Keller, Impact of plasma-induced surface chemistry on electrochemical properties of microfabricated pyrolytic carbon electrodes, Electrochim. Acta 410 (2022) 139987.
[46] S.Y. Lee, G.R. Choi, H. Lim, K.M. Lee, S.K. Lee, Electronic transport characteristics of electrolyte-gated conducting polyaniline nanowire field-effect transistors, Appl. Phys. Lett. 95 (2009) 013113.
[47] D. Vanmaekelbergh, A.J. Houtepen, J.J. Kelly, Electrochemical gating: a method to tune and monitor the (opto)electronic properties of functional materials, Electrochim. Acta 53 (2007) 1140–1149.
[48] J. Li, P.H.Q. Pham, W. Zhou, T.D. Pham, P.J. Burke, Carbon-nanotube–electrolyte interface: quantum and electric double layer capacitance, ACS Nano 12 (2018) 9763–9774.
[49] J.D. Wiggins-Camacho, K.J. Stevenson, Effect of nitrogen concentration on capacitance, density of states, electronic conductivity, and morphology of N-doped carbon nanotube electrodes, J. Phys. Chem. C 113 (2009) 19082–19090.
[50] S.J. Prestrelski, N. Tedeschi, T. Arakawa, J.F. Carpenter, Dehydration-induced conformational transitions in proteins and their inhibition by stabilizers, Biophys. J . 65 (1993) 661–671.
[51] L.A. Zacharoff, M.Y. El-Naggar, Redox conduction in biofilms: from respiration to living electronics, Curr. Opin. Electrochem. 4 (2017) 182–189.
[52] N.L. Ing, T.D. Nusca, A.I. Hochbaum, *Geobacter sulfurreducens* pili support ohmic electronic conduction in aqueous solution, PCCP 19 (2017) 21791–21799.
[53] M.F.G. Velho, R.A.L. Silva, D. Belo, The quest for single component molecular metals within neutral transition metal complexes, J. Mater. Chem. C 9 (2021) 10591–10609.
[54] S. Giannini, A. Carof, M. Ellis, H. Yang, O.G. Ziogos, S. Ghosh, J. Blumberger, Quantum localization and delocalization of charge carriers in organic semiconducting crystals, Nat. Commun. 10 (2019) 3843.
[55] J.R. van der Veen, S. Valianti, H.S.J. van der Zant, Y.M. Blanter, F.J.R. Meysman, A model analysis of centimeter-long electron transport in cable bacteria, PCCP 26 (2024) 3139–3151.